



Singular spectrum analysis-based hybrid PSO-GSA-SVR model for predicting displacement of step-like landslides: a case of Jiuxianping landslide

Haijia Wen¹ · Jiafeng Xiao¹ · Xuekun Xiang^{1,2} · Xiongfeng Wang¹ · Wengang Zhang¹

Received: 20 November 2022 / Accepted: 3 August 2023 / Published online: 4 September 2023
© The Author(s), under exclusive licence to Springer-Verlag GmbH Germany, part of Springer Nature 2023

Abstract

As the displacement of step-like wading landslides is highly nonlinear and complex, it is difficult to develop a reasonable and accurate prediction model. Effective prediction of landslide displacement depends on the performance of the prediction model and the quality of monitoring data, which is greatly affected by sudden rainstorm and flood. To improve the prediction accuracy of the study model, Global Navigation Satellite System (GNSS) is used to monitor surface displacement. The GNSS-based displacement data are used to develop a hybrid model by combining Particle Swarm Optimization (PSO), Gravitational Search Algorithm (GSA) and Support Vector Regression (SVR). The displacement of Jiuxianping landslide, a typical wading rock landslide in Yunyang, China, has obvious step-like distribution characteristic. Firstly, the deformation characteristics and failure modes of Jiuxianping landslide are inductively analyzed. The step-like landslide displacement is decomposed into trend term and periodic term after reducing data noise by singular spectrum analysis (SSA). Then, a polynomial fitting model for the trend term prediction is developed, while multi-models are developed by PSO-SVR, GSA-SVR and PSO-GSA-SVR for predicting the periodic term. The three models were compared, and the sequence of removing the random term was evaluated again after it was reconstructed. Finally, the cumulative displacement was obtained by superimposing the trend displacement and the periodic displacement. Also, it was compared with the actual monitoring displacement. The results show that: (1) the step-like phenomenon of landslide displacement is mainly affected by rainfall and reservoir water level (RWL), and the displacement of the abrupt segment of the landslide exhibits an overall convex deformation; (2) SSA could effectively decompose the highly nonlinear step-like landslide displacement into trend term and periodic term; (3) the correlation coefficient of the hybrid-optimized PSO-GSA-SVR model for predicting the periodic displacement is more than 0.85, and the correlation coefficient of the overall displacement prediction model is 0.99. This work provides a better displacement prediction model for predicting a typical step-like wading rock landslide.

Keywords Displacement prediction · PSO-GSA-SVR · Singular spectrum analysis · Step-like · Wading rock landslide

1 Introduction

Landslide is one of the most common natural disasters worldwide, particularly in reservoir banks and mountainous areas, posing a significant threat to human life and loss of their properties [10, 30]. With the rapid economic development in China, the construction of hydropower projects has become a top priority. The Three Gorges Reservoir (TGR) project in China is a prominent example of such a project. Due to the complex geological environment, the TGR is susceptible to numerous rock mass movements. Based on an incomplete survey,

✉ Haijia Wen
jhw@cqu.edu.cn

¹ Key Laboratory of New Technology for Construction of Cities in Mountain Area of the Ministry of Education, National Joint Engineering Research Center for Prevention and Control of Environmental GeoHazards in the TGR Area, School of Civil Engineering, Chongqing University, Chongqing 400045, China

² Chongqing Institute of Geology and Mineral Resources, Chongqing 400042, China

approximately 5000 landslides have occurred since the initial impoundment of the TGR Dam in 2003, with around 3000 of them being wading rock landslides [13, 33, 34]. Landslides are more prone to creep and sudden change with RWL variation or rainfall [29, 37, 44].

In recent years, many scholars have analyzed and predicted the occurrence of landslides caused by both rainfall and RWL [19, 24]. They have also proposed some effective models for landslides prediction [28, 32]. Currently, these methods employed for analyzing landslide displacement mainly involve laboratory physical model tests and time series machine learning model [26]. The laboratory physical model is derived from a wide range of actual observed creep tests. It has a solid physical foundation and can be used for effective prediction of landslides. However, this model has strict limitations [11, 23, 33]. With the development of computer technology, nonlinear machine learning models based on nonlinear theory have been gradually developed, including traditional nonlinear models [17], neural networks [4, 14], XGboost [42, 43], SVR [3, 22, 31, 45] and extreme learning machines [1]. As science and technology gradually improved, artificial intelligence scientific algorithm began to flourish, which in turn led to the fruitful results obtained from the prediction of landslide displacement. Zhang [39] applied an advanced deep machine learning method-gated recurrent unit (GRU) to predict the displacement of Jiuxianping landslide in Yunyang County, Chongqing. Zhou and Yin [45] used the displacement of Bazimen landslide, in TGR, as an example to study typical step-like landslides displacement. Based on the time series theory, the average movement method was used to divide the total displacement of Bazimen landslide into trend items and periodic items. Polynomial fitting method and PSO-SVM model were used for its prediction. Han and Shi [7] used Support Vector Classification (SVC) to classify and identify the displacement of Majiagou landslide and used PSO-SVR to predict its abrupt displacement section. Single intelligent optimization algorithm used for data processing leads to incomplete identification, easy to local optimization, slow convergence and stagnation, which result in large errors. Multiple hybrid models have stronger prediction and improved generalization ability [38, 40, 46]. Single optimization algorithm needs to be improved, so it is necessary to apply hybrid intelligent optimization algorithm model [43].

From the displacement monitoring curve, landslides can be divided into four categories: stable-type landslides, exponential-type landslides, step-like landslides and convergence-type landslides [22]. For the displacement of step-like deformation of wading rock landslides, there are more unpredictable disasters, and it has been a hot issue [16, 20]. Landslide displacement prediction is mainly divided into three stages: empirical prediction stage,

statistical prediction stage and nonlinear prediction stage [38]. In the nonlinear prediction stage, the total displacement of landslides accumulates periodic displacement by trend displacement. The trend term is always controlled by the internal evolution of the landslide and its own conditions, and the periodic term is induced by external factors, such as rainfall, RWL, etc. [35]. The trend displacement is predicted by function fitting method, and the periodic displacement can be predicted by machine learning methods [12]. Choosing a reasonable and fast method for decomposing the total displacement is the primary factor in verifying its reliability [9]. Displacement time series decomposition methods include moving average method, double exponential smoothing (DES), discrete wavelet transform (DWT), empirical mode decomposition (EMD), etc. [15]. Filter method is simple, but it needs to determine the trend item type. Wavelet method does not need to determine the trend, but it needs to estimate the basic function in advance. The process of smoothing method is simple, but the parameter selection is complex, and the displacement of trend term is step-like. Empirical mode method can easily be used to mix different modal signals [3, 21]. SSA is a method that deals with nonlinear time series data. It has no model, does not require stationary time series and does not assume a parametric model. It can be widely used in various time series. The time series to be studied are decomposed and reconstructed to identify different signals in the original sequence, so as to extract the trend term, periodic term, etc. [25]. However, field monitoring data sets are often contaminated and highly nonlinear. Golyandina [6] used a case to demonstrate SSA combined with R for analysis, prediction and parameter estimation, proving that SSA is a powerful tool for analyzing and predicting time series. In this context, Zhang and Wang [36] combined SSA with support vector machine (SVM) and cuckoo search (CS) algorithm. Compared with other methods (SVM, CS-SVM, SSA-SVM, SARIMA and BPNN), they found that the model can significantly improve the accuracy of forecasting short-term power load. Liu [18] proposed a novel multistep wind speed prediction model by combining Variational Mode Decomposition (VMD), SSA, Extreme Learning Machine (ELM) and a forecasting model. The wind speed is decomposed into several sub-layers, and it is found that the prediction speed of the sub-layer is fast and the generalization performance is good. Based on the aforementioned findings, this study combines SSA method with intelligent optimization algorithm, and achieves remarkable results in the field of short-term power load forecasting, medical forecasting and weather forecasting. However, it is less used in landslide disaster forecasting and has application prospects.

In summary, this paper uses Jiuxianping wading rock landslide as an example to analyze the displacement of

step-like landslides. Firstly, the deformation characteristics and failure modes of the landslide are analyzed for the monitoring data set. Then, the SSA algorithm is used to decompose the landslide monitoring displacement, remove the random signal and extract the trend displacement and periodic displacement. After the SSA algorithm was reconstructed, it was evaluated to prove that the trend term and periodic term are reasonable enough after they were randomly decomposed. For the evaluation of the trend term using power function polynomial fitting prediction, the periodic displacement is trained and tested by the improved GSA-PSO and SVR model. Finally, the trend term and the periodic displacement are accumulated and compared with the actual monitoring displacement. The mean absolute error (MAE), mean square error (MSE) and correlation coefficient (R) are used as evaluation indexes to prove the feasibility of the method. This idea provides a new intelligent algorithm for predicting landslide displacement and it can be used as a new reference for predicting and providing early warnings about the occurrence of landslides.

2 Research areas and data

2.1 Jiuxianping landslide and geological environment

Jiuxianping landslide is located on the left bank of the Yangtze River in the lower reaches of Yunyang County, Chongqing. It is found in the TGR area, 239 km away from the dam site. It is a typical wading rock landslide. The coordinates of the center point are $108^{\circ} 46' 57.35''$ E, $30^{\circ} 56' 27.63''$ N. The main sliding direction is 144° , the length is about 1200 m, the middle width is about 850 m, the average thickness is 40 m, the area is $144 \times 104 \text{ m}^2$ and the volume is about $5700 \times 104 \text{ m}^3$. The boundary is roughly fan-shaped, and can be seen in the UAV orthographic projection (Fig. 1).

The bedrock orientation at the trailing edge of the Jiuxianping landslide is $137^{\circ} \angle 24^{\circ}$, while the leading edge of the Jiangbian landslide exhibits an orientation of $326^{\circ} \angle 9^{\circ}$. This region features an erosion-prone low mountain valley landform, with higher elevations in the northeast gradually declining towards the southwest. The ground elevation ranges from 134 to 587 m, with a relative height difference of 453 m. The angle between the flow direction of the Yangtze River and the strike of the underlying bedrock strata ranges from 40° to 60° , resulting in an oblique slope shape. Generally, the longitudinal terrain is characterized by gentle slopes or platform-like features. The leading edge of the Jiuxianping landslide extends 145 m below the water level of the Yangtze River, indicating a wading landslide. The annual RWL before

dam fluctuations ranges between 145, 175 and 145 m, significantly impacting the stability of the landslide due to RWL changes.

2.2 Deformation characteristics and failure modes

According to the description from site, many cracks appeared during this period, mainly tensile cracks, followed by shear cracks. Chongqing Institute of Geology and Mineral Resources conducted a detailed investigation of the area, and observed surface cracks on the landslide, up to 1 m deep and 0.5 m wide (Fig. 2c), tensile cracks clearly visible on the cement floor of residential courtyard and Concrete pavement (Fig. 2a and b), shear cracks and other macroscopic cracks on the wall of the house (Fig. 2a and d), and the bare rock of the wading part, which shows bedding rock (Fig. 2e). For wading rock landslides, in addition to the sliding body, sliding zone, free deformation space, internal and external forces, the primary condition for sliding deformation is to have lateral boundary and trailing edge boundary conditions. Under the action of structure, creep or slip deformation, the trailing edge boundary condition of tension crack is formed. The front edge of landslide is free, and the trailing edge is bounded by tension crack groove and slope top.

Based on the above investigation and analysis, the landslide failure mode is slip-bending, which mainly occurs in the bedding slope. When the dip angle of the rock layer in the bank slope is steeper than the slope of the bank itself, indicating a steep dip in the same direction, and the dip angle of the sliding surface exceeds the comprehensive friction angle of the surface, the overlying rock mass possesses the conditions necessary to slide along the sliding surface. However, the sliding surface is not free, preventing its sliding. Under certain conditions, there could be bending deformation of the middle and lower rock mass until there is buckling failure. Generally, it can be divided into three stages: bending stage, uplift stage and penetration stage. During the deformation process, a certain amount of elastic strain energy is stored in the bending part. Therefore, once the lower sliding body starts, the release of elastic strain energy can accelerate the additional thrust of the sliding body.

2.3 Monitoring scheme and result analysis

The conditioning factor of the landslide is the early tectonic movement, which leads to the development of sandstone joints during the formation of syncline. The weak surface (belt) and main sliding surface (belt) are produced in the contact surface of sand mudstone and mudstone strata. The new tectonic movement, crustal

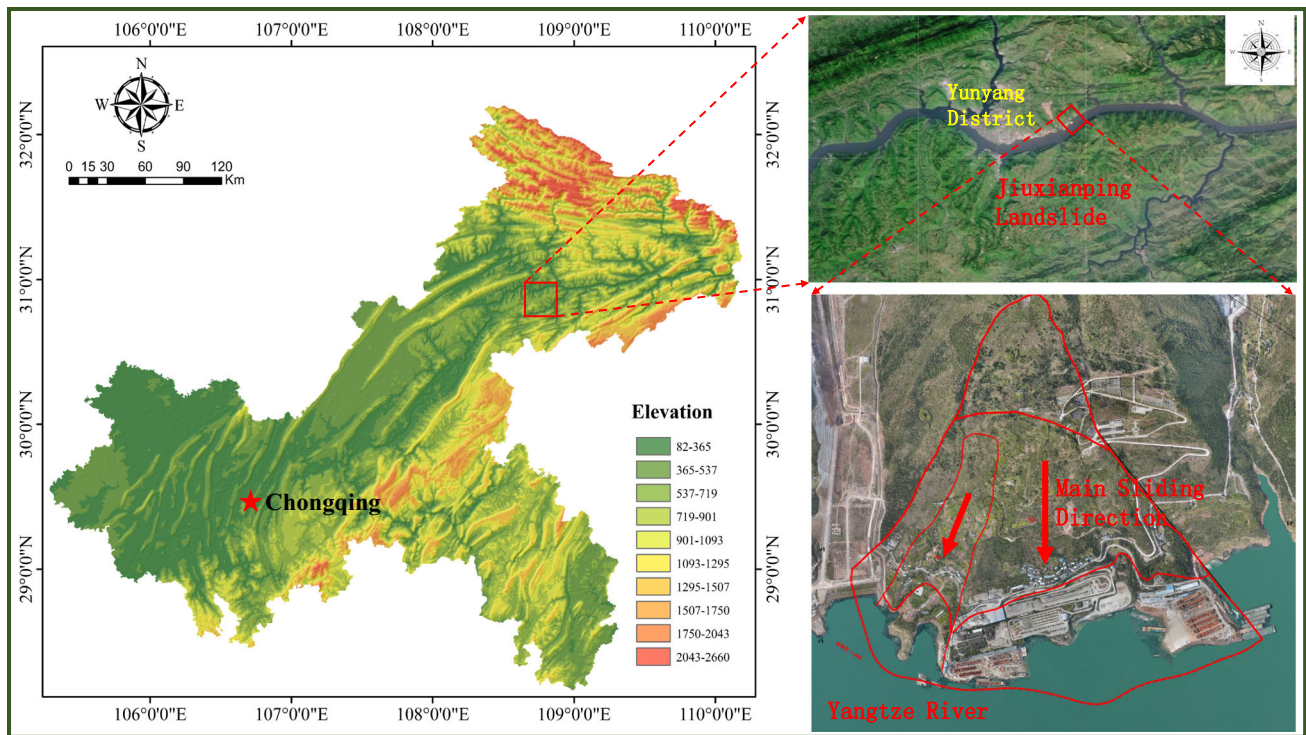


Fig. 1 Location of Jiuxianping landslide and UAV orthophoto

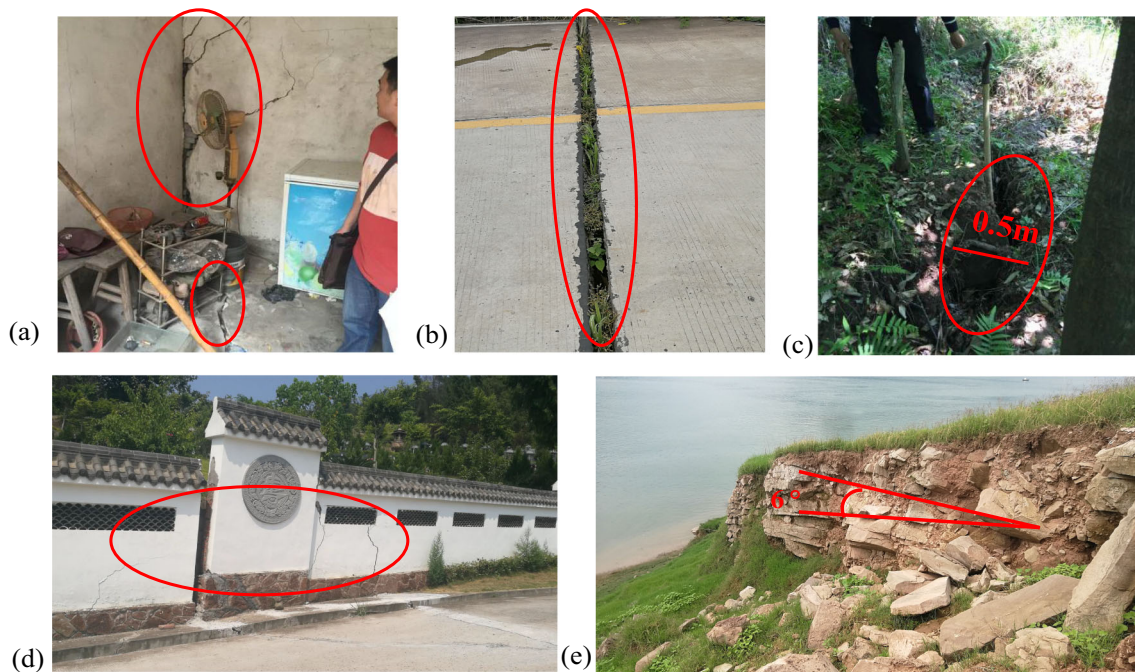


Fig. 2 Jiuxianping landslide deformation characteristics: **a** house deformation characteristics, **b** road deformation characteristics, **c** landslide trailing edge tensile cracks, **d** wall deformation characteristics, **e** landslide front edge bare rock

uplift, river incision, the leading edge of the free landslide along the sliding deformation provide deformation space. The triggering factors of landslides are rainstorm or

extreme rainfall and RWL fluctuation. The primary factor that causes the instability of landslides is RWL fluctuation.

The landslides displacement in the TGR area have step-like characteristics, and the short-term deformation of

landslides is affected by RWL and rainfall. In the stage of landslide mutation, the displacement–time curve of landslide deformation evolution stage has three obvious processes: initial deformation stage, constant deformation stage and accelerated deformation stage [22]. Therefore, it is particularly important to identify the stages of landslide displacement to warn against disaster. To understand landslide deformation in the area, Jiuxianping landslide monitoring network is arranged for real-time and accurate monitoring (Fig. 3). In this paper, the II–II' section is taken as the research object (Fig. 4), and the monitoring data and geological data of the section are selected correspondingly.

To facilitate the study of step-like displacement in the main sliding direction, the landslide surface displacement data collected by YY208, YY209 and YY210 displacement monitoring stations are selected for research. From Fig. 5, the displacement of the three monitoring points showed

step-like-change, the periodic law is obvious, and it is easy to study the relationship between displacement and rainfall and RWL.

The rainfall of Jiuxianping landslide is most vigorous in summer and autumn, and the regulation of RWL shows obvious periodicity (Fig. 5). Under the combined action of RWL drop and rainstorm, the displacement of landslide has obvious step-like phenomenon (Fig. 5). The rise of RWL leads to stable deformation of the landslide. The decrease of RWL has sudden change on the landslide, and there is an obvious lag effect. When RWL rises, the RWL between 160 and 175 m points to the hydrodynamic pressure inside the landslide, which enhances the stability of the landslide. When RWL drops, the RWL is between 160 and 145 m and produces hydrodynamic pressure pointing out of the slope and downward. This accelerates the deformation of the landslide. The time point at which mutation of the

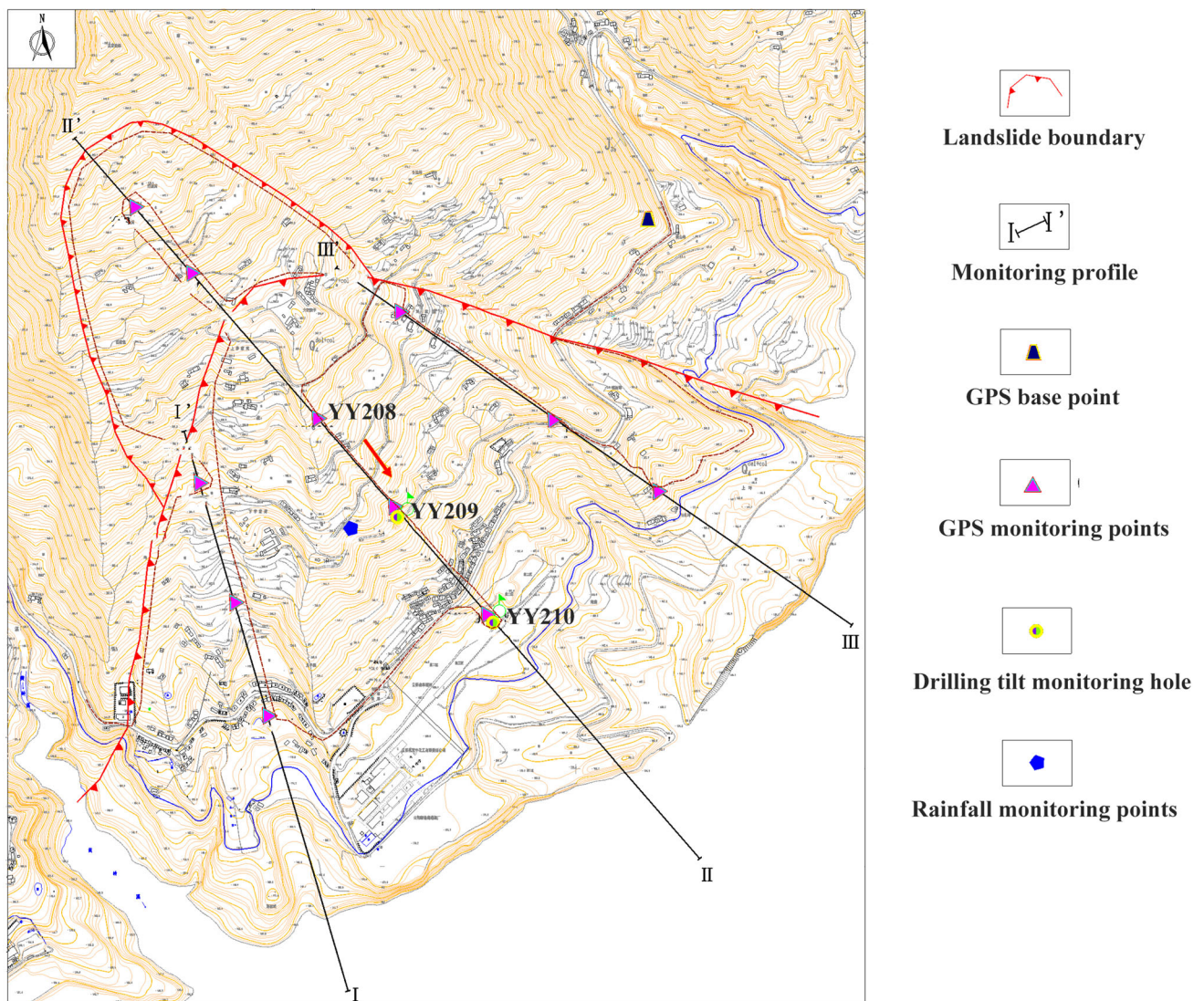


Fig. 3 Jiuxianping landslide monitoring network

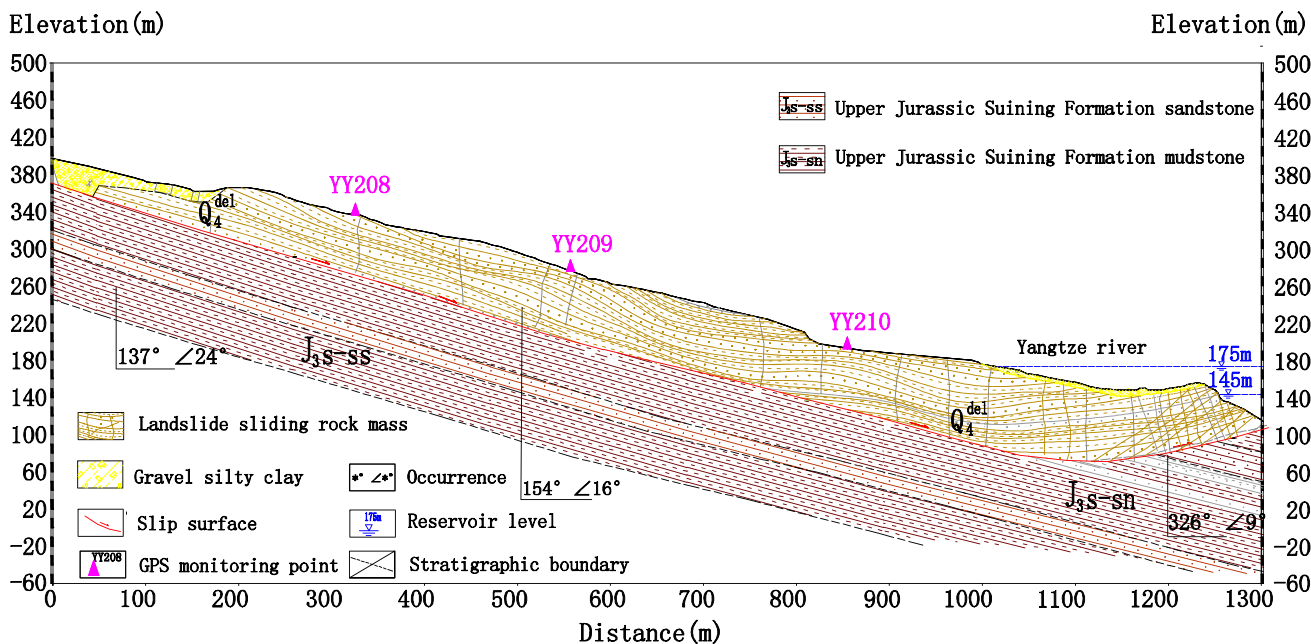


Fig. 4 II-II' profile and displacement monitoring layout

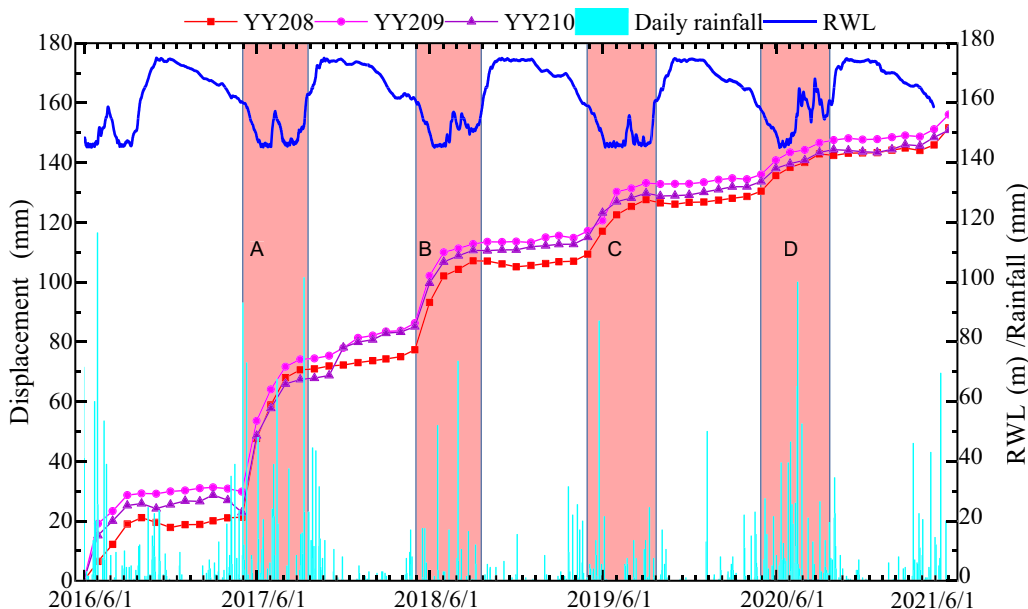


Fig. 5 RWL (m), Rainfall (mm) and Displacement (mm) of II-II' landslide profile

landslide displacement occurs each year is the low RWL point, and each may belong to the accelerated deformation stage (Fig. 6).

Rainfall is also one of the factors that lead to landslide displacement. September to October 2017 were a dense rainfall period during autumn; there was relatively heavy rainfall, and the RWL increased (the dynamic water pressure pointed to the landslide interior to stabilize the landslide). However, the monitoring point YY210 near the water end of the RWL has a large mutation displacement.

The sudden displacement that occurred in November 2017 occurred during a period of high RWL and without heavy rainfall. This indicates a lag effect in rainfall, with a relatively long delay. Furthermore, it can be observed that the infiltration of rainfall (due to material properties and slow seepage) leads to much slower changes in pore water pressure compared to the decrease in the RWL (Fig. 5). Based on the above, the deformation of landslide is affected by RWL level and rainfall. RWL plays a major role in the displacement and deformation of landslide, but

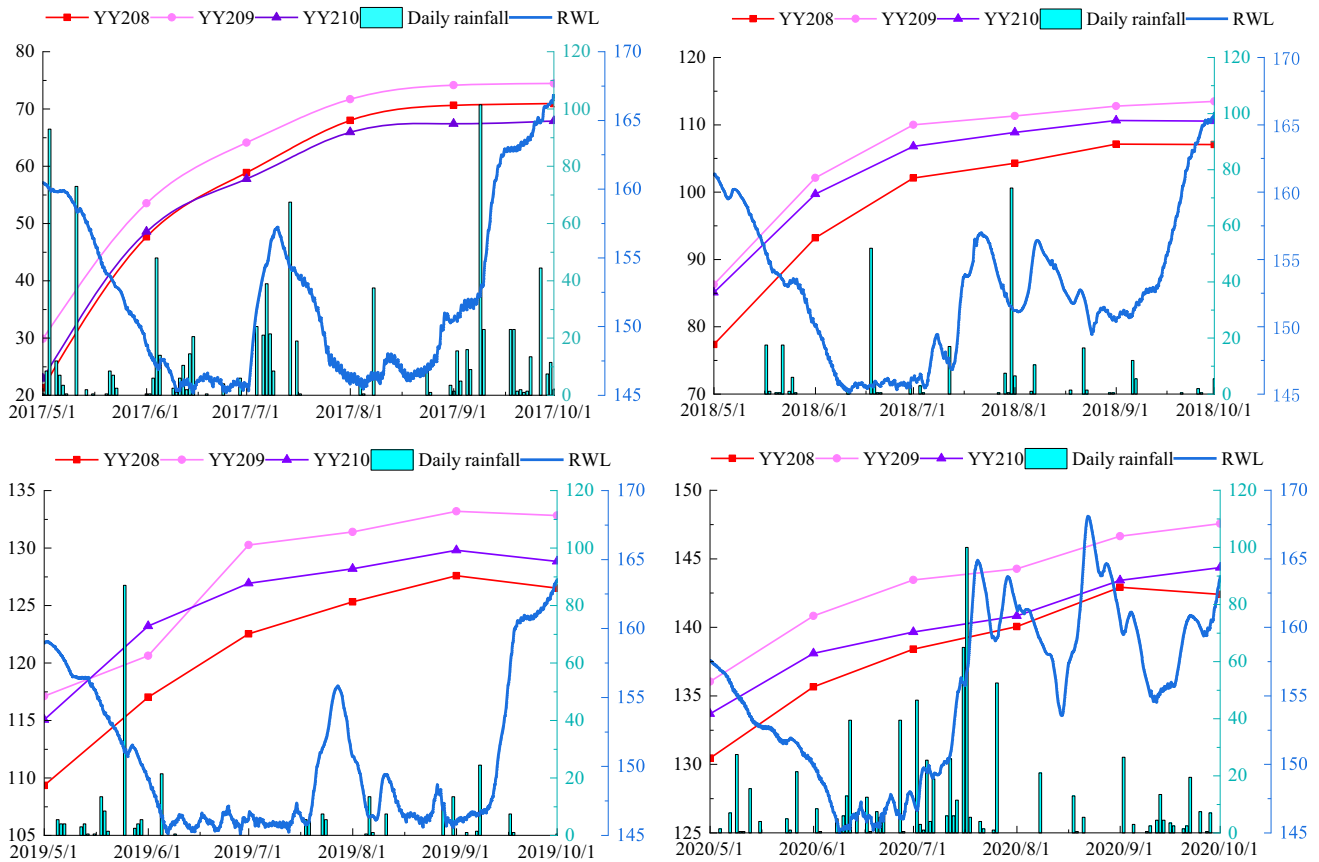


Fig. 6 A, B, C and D detail of regional monitoring data

the influence of rainfall cannot be ignored. Based on this, RWL and rainfall are selected as influencing factors.

The triggering of landslides (Segments A, B, C and D) is induced by rainfall. The cumulative displacement of the transitional segment exhibits an overall convex deformation. Under the interaction of RWL and rainfall, low RWL correspond to convex deformation displacement, while heavy rainfall corresponds to concave deformation displacement (Fig. 6).

3 Method and model developing

3.1 SSA

The steps are as follows[8]:

(1) Embed

Assume that the one-dimensional displacement data time series is $X = (x_1, x_2, \dots, x_N)$, $1 < L < N$. The positive integer L is the length of the sliding window, where sampling is equally spaced and the length is N . One-dimensional displacement data is mapped into a multi-

dimensional trajectory matrix, which is a Hankel matrix and can be expressed:

$$X = \begin{bmatrix} x_1 & x_2 & x_3 & \dots & x_K \\ x_2 & x_3 & x_4 & \dots & x_{K+1} \\ \vdots & \vdots & \vdots & \ddots & \vdots \\ x_L & x_{L+1} & x_{L+2} & \dots & x_N \end{bmatrix} \tag{1}$$

where L is the embedding dimension, and $X_i = [x_i, x_{i+1}, \dots, x_{i+L-1}]$. Each element of the matrix is equal diagonally.

(2) Decomposition

Calculate XX^T and obtain L eigenvalues $\lambda_1, \lambda_2, \dots, \lambda_L$; U_1, U_2, \dots, U_L is the orthogonal eigenvectors corresponding to the eigenvalues. $L = \max(L, \lambda_i > 0) = R(A)$, then the following equation is obtained:

$$\left. \begin{aligned} X &= X_1 + X_2 + \dots + X_L \\ X_i &= \sqrt{\lambda_i} U_i V_i^T \\ V_i &= X^T U_i / \sqrt{\lambda_i} (i = 1, 2, \dots, L') \end{aligned} \right\} \tag{2}$$

where X_i is the elementary matrix, $\sqrt{\lambda_i}$ is the singular value of matrix X , U_i is the empirical orthogonal function of matrix X , V_i is the main component of matrix X , and $\sqrt{\lambda_i}$, U_i and V_i is the i th triple eigenvector of matrix X .

(3) Grouping

The matrices contained in each group are added, as shown in the following:

$$\left. \begin{aligned} X &= X_{I_1} + X_{I_2} + \dots + X_{I_m} \\ X_I &= X_{i_1} + X_{i_2} + \dots + X_{i_p} \end{aligned} \right\} \quad (3)$$

where the contribution rate of X_i is $\alpha = \lambda_i / \sum_{i=1}^L \lambda_i$.

(4) Reconfiguration

The reconstructed sequence can be obtained by the following:

$$\left. \begin{aligned} y_{rc_k} &= \frac{1}{k} \sum_{m=1}^k y_{m,k-m+1}^* & 1 \leq k < L^* \\ y_{rc_k} &= 1/L^* \sum_{m=1}^{L^*} y_{m,k-m+1}^* & L^* \leq k \leq K^* \\ y_{rc_k} &= \sum_{m=k-K^*+1}^{N-K^*+1} y_{m,k-m+1}^* / N - k + 1 & K^* < k \leq N \end{aligned} \right\} \quad (4)$$

3.2 PSO-GSA

In GSA, the definition of the gravitational mass of the particle and the updating formula of the inertial mass are obtained from the fitness function in the following equation [5]:

$$\left. \begin{aligned} M_i(t) &= \frac{m_i(t)}{\sum_{j=1}^N m_j(t)} \\ m_i(t) &= \frac{f_i t_i(t) - f_{\text{worst}}(t)}{f_{\text{best}}(t) - f_{\text{worst}}(t)} \end{aligned} \right\} \quad (5)$$

where, $f_i t_i(t)$ is the moderate function value of particle i at time t , and the MSE of SVR is taken as the fitness function; $f_{\text{best}}(t)$ and $f_{\text{worst}}(t)$ are the best and worst fitness function values of the group at time t . Gravity mass is generally expressed in units of $M_i(t)$.

After using the PSO-GSA, the calculation formulas of the resultant force $F_i^k(t)$, acceleration $\alpha_i^k(t)$, position $X_i^k(t)$ and velocity $V_i^k(t)$ of the k -dimensional particle i are updated as follows [27]:

$$\left. \begin{aligned} F_i^k(t) &= \sum_{j=1, j \neq i}^N \lambda F_{ij}^k(t) \\ \alpha_i^k(t) &= \frac{F_i^k(t)}{M_i(t)} \\ V_i(t+1) &= \omega V_i(t) + c_1 r_1 a c_i(t) \\ &\quad + c_2 r_2 (P_{\text{best}} - X_i(t)) \\ X_i(t+1) &= X_i(t) + V_i(t+1) \end{aligned} \right\} \quad (6)$$

where λ is a random number in $[0, 1]$, β is a uniform random distribution in $[0, 1]$, and k is the dimension space.

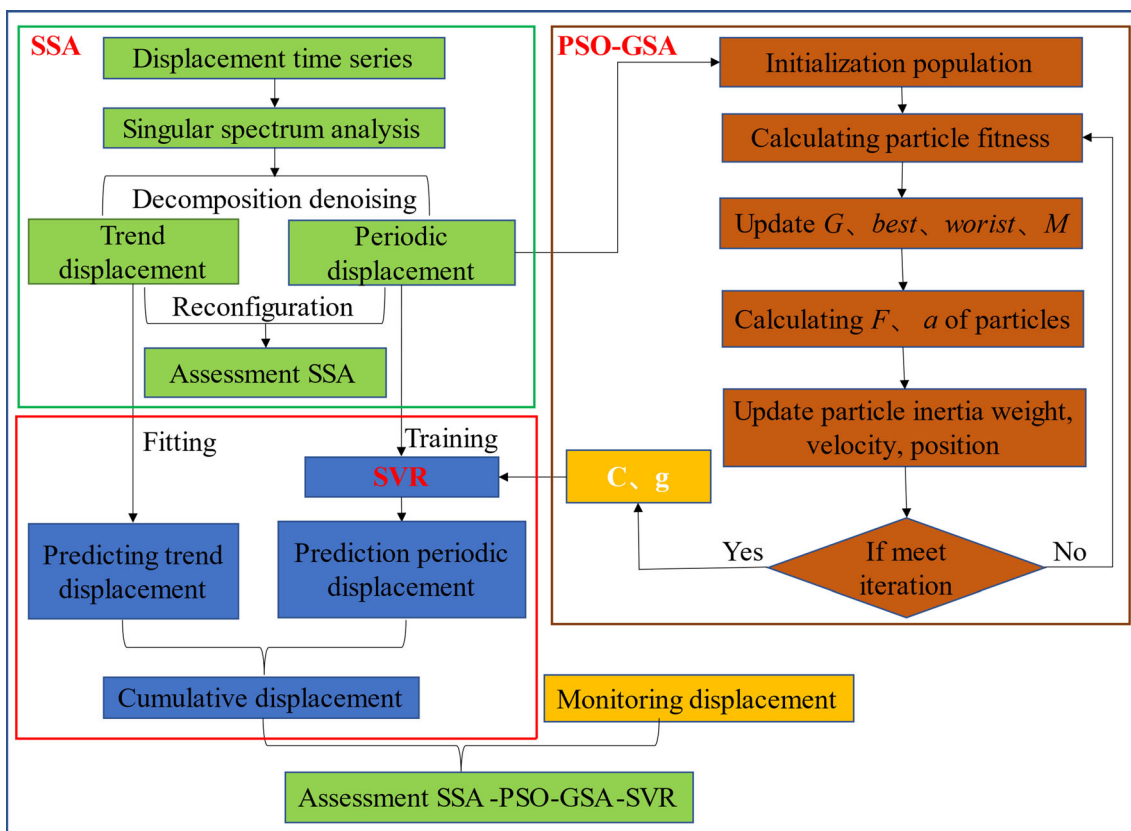


Fig. 7 Flowchart of the prediction method

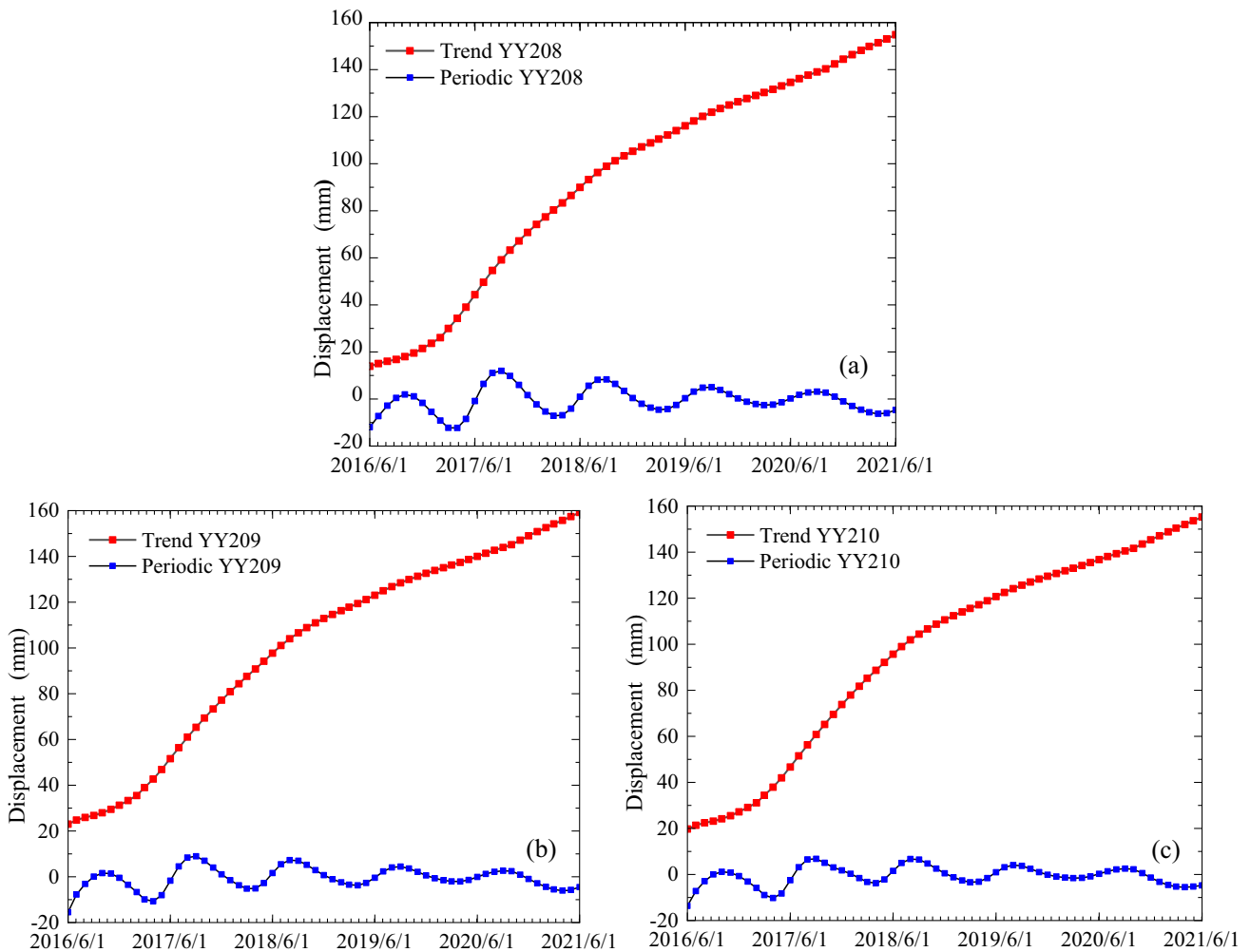


Fig. 8 Trend and periodic terms after SSA decomposition results: **a** YY208, **b** YY209, **c** YY210

c_1 and c_2 are constants in $[0, 1]$, r_1 and r_2 are random numbers between $[0, 1]$, P_{best} is the local optimal value and ω is the inertia weight.

3.3 SVR

The optimal regression function is given in the following equation [41]:

$$f(x) = \omega^T x + b \tag{7}$$

where ω is the weight vector, b is the bias vector. The prediction data $f(x_i)$ is obtained according to the input influencing factor x_i . By introducing the relaxation factor, the objective optimization function of SVR is given in the following equation:

$$\left. \begin{aligned} & \min \frac{1}{2} \|w\|^2 + C \sum_{i=1}^m (\xi_i + \xi_i^*) \\ & \text{s.t. } \left. \begin{aligned} & f(x_i) - y_i \leq \varepsilon + \xi_i \\ & y_i - f(x_i) \leq \varepsilon + \xi_i^* \\ & \xi_i \geq 0, \xi_i^* \geq 0, i = 1, 2, \dots, m \end{aligned} \right\} \end{aligned} \tag{8}$$

where C is the penalty function, ε is the maximum regression error, ξ_i and ξ_i^* is the slack variable. By introducing a Gaussian radial basis (RBF) kernel function: $K(x_i, x_j) = \exp(-\|x - x_i\|^2 / 2g^2)$ and Lagrange multiplier α_i^* and α_i , the prediction regression equation is written again in the following equation:

$$f(x) = \sum_{i=1}^m (\alpha_i^* - \alpha_i) K(x_i, x_j) + b \tag{9}$$

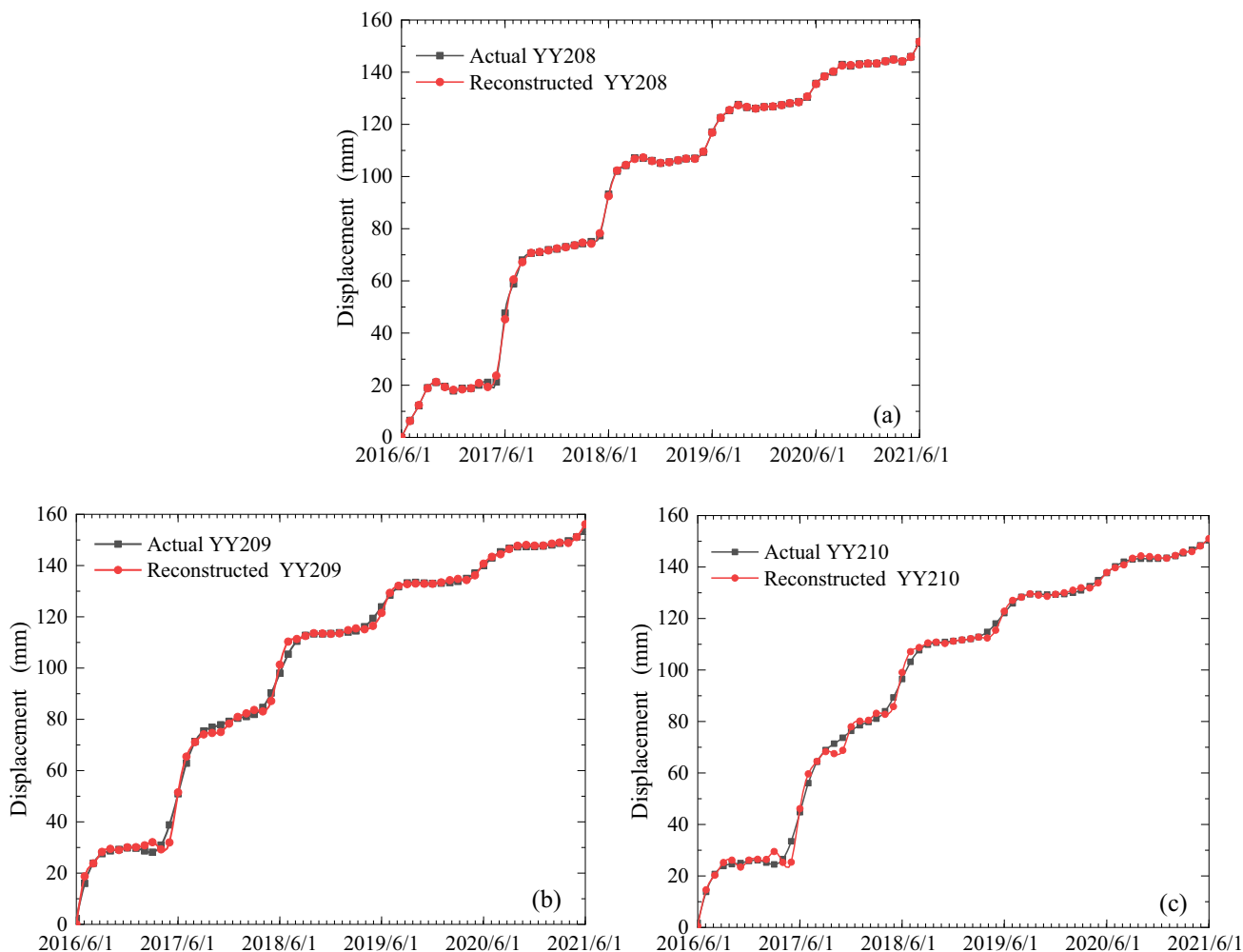


Fig. 9 Comparison of time series of actual displacement and reconstructed displacement results: a YY208, b YY209, c Y210

Table 1 Evaluation of reconstructed sequence and actual displacement fitting results

	MSE (mm ²)	MAE (mm)	R
YY208	0.357	0.331	0.999
YY209	0.332	0.359	0.999
YY210	0.438	0.397	0.999

Table 2 Polynomial coefficient

	a_0	a_1	a_2
YY208	1.528	4.364	− 0.032
YY209	11.18	4.231	− 0.031
YY210	6.532	4.346	− 0.033

3.4 Model developing and validation

The calculation flow chart of the SSA-PSO-GSA-SVR model is shown in Fig. 7. Each monitoring displacement in time series is composed of several factors. After removing the influencing random factors, Jiuxianping landslide displacement is decomposed into trend term and periodic displacement by SSA algorithm. Therefore, the cumulative displacement is expressed as follows:

$$s_t = u_t + v_t \tag{10}$$

where S_t is the cumulative displacement time series of landslide displacement, u_t is the trend displacement series and v_t is the periodic displacement series. The cumulative displacement of the landslide can be obtained by superimposing the trend displacement and the periodic displacement.

The trend term is always controlled by the internal evolution of the landslide and its own conditions, and the periodic term is induced rainfall and RWL. The trend term

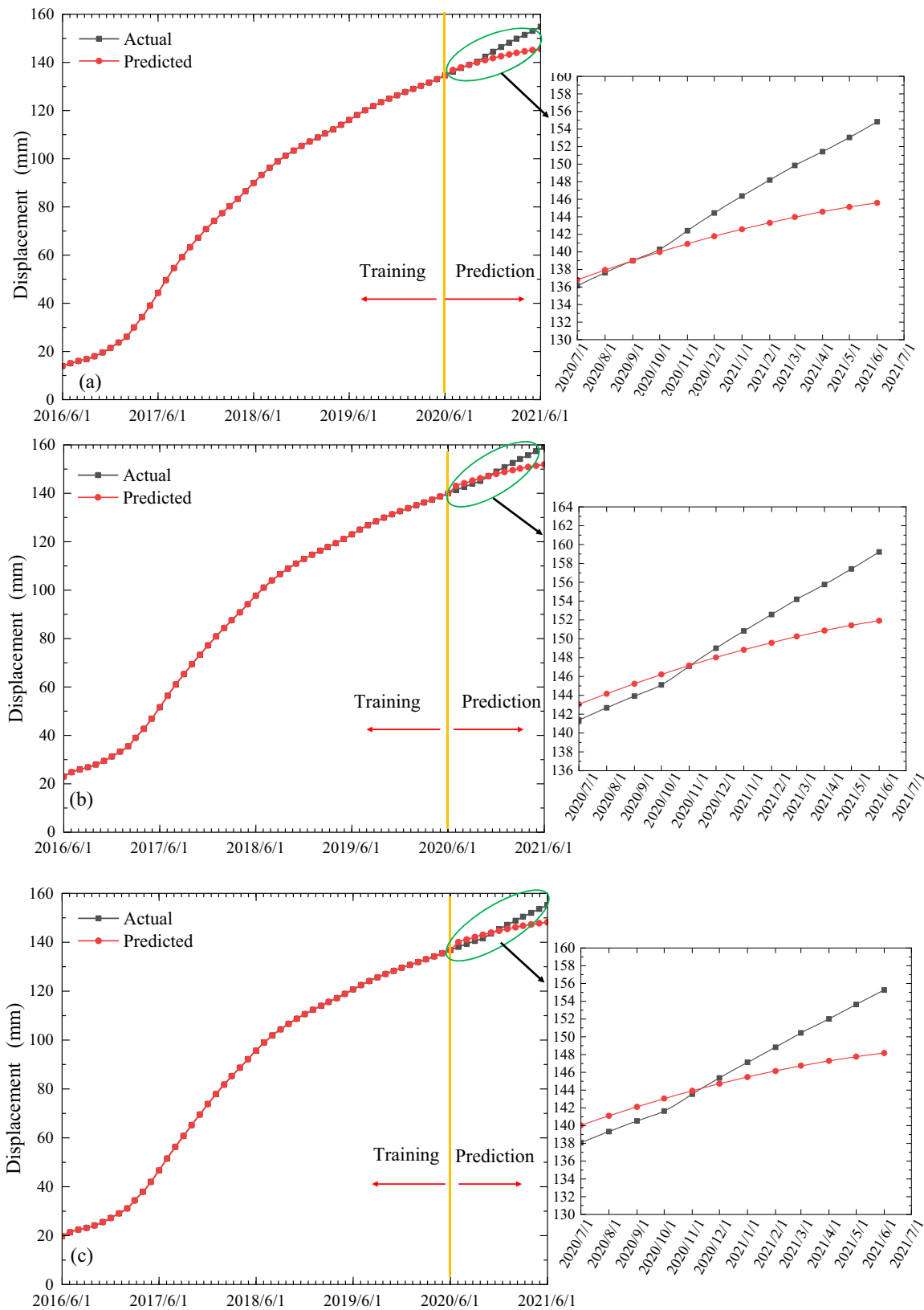


Fig. 10 The displacement–time curve of the three monitoring points trend prediction results: **a** YY208, **b** YY209, **c** YY210

Table 3 Evaluation of trend displacement prediction results

	MSE (mm ²)	MAE(mm)	R
YY208	23.121	3.664	0.989
YY209	12.539	2.811	0.988
YY210	11.889	2.787	0.984

is fitted and predicted by multiple polynomials, and the periodic term is trained and predicted by PSO-GSA-SVR algorithm. Finally, the cumulative displacement is evaluated.

In this paper, mean absolute error (MAE), mean square error (MSE) and correlation coefficient (*R*) are used to evaluate the error of the model in the following:

$$\left. \begin{aligned} \text{MAE} &= \sum_{i=1}^n (x - x_i) / n \\ \text{MSE} &= \sum_{i=1}^n (x - x_i)^2 / n \end{aligned} \right\} \quad (11)$$

$$R = \frac{\sum_{i=1}^N (x_i - \bar{x})(\hat{x}_i - \bar{\hat{x}})}{\sqrt{\sum_{i=1}^N (x_i - \bar{x})^2} \sqrt{\sum_{i=1}^N (\hat{x}_i - \bar{\hat{x}})^2}} \quad (12)$$

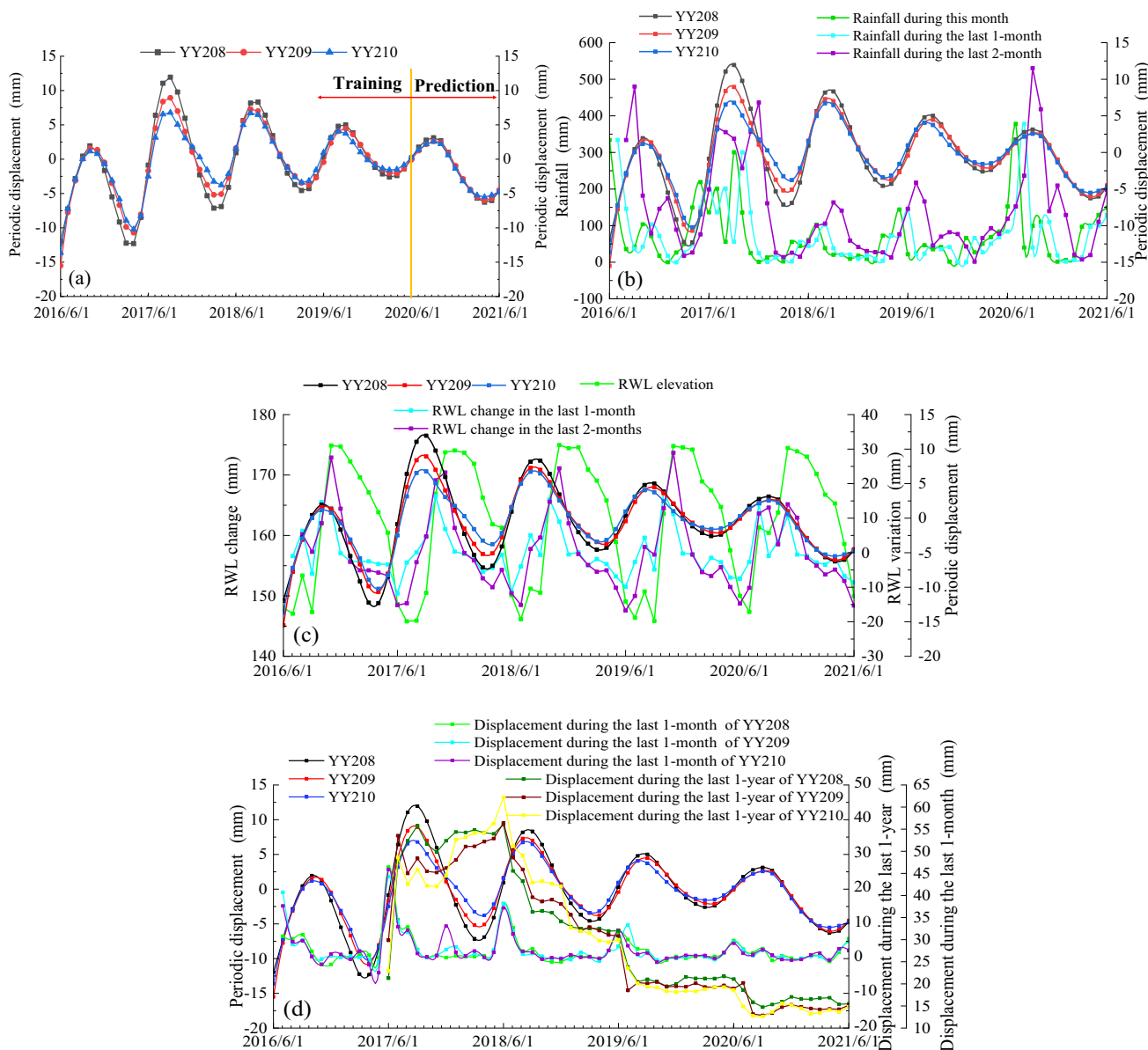


Fig. 11 a Periodic displacement. b Relationship between rainfall and periodic displacement. c Relationship between RWL, RWL change and periodic displacement. d Relationship between annual displacement, monthly displacement and periodic displacement

Table 4 Relationship between periodic displacement and eight influence factors

Impact factors	YY208	YY209	YY210
Rainfall during this month	0.767	0.767	0.767
Rainfall during the last 1-month	0.773	0.771	0.771
Rainfall during the last 2-months	0.712	0.711	0.711
RWL elevation	0.892	0.902	0.901
RWL change in the last 1-month	0.632	0.682	0.684
RWL change in the last 2-months	0.697	0.692	0.711
Displacement during the last 1-year	0.724	0.7	0.709
Displacement during the last 1-month	0.751	0.782	0.794

where x is the measured value, x_i is the predicted value and n is the sample size. The lower the MAE and MSE, the higher the predictive intensive reading; the closer R is to 1, the stronger the correlation.

4 Results and discussion

4.1 Decomposition and reconstruction of trend and periodic terms

In order to simultaneously verify the feasibility of the proposed method, three monitoring points are selected. The time series data of YY208, YY209 and YY210 displacement monitoring points are decomposed by SSA. SSA is used to analyze the data for classification and dimension transformation. There are 3 monitoring point data (each monitoring point for 60 months) for trend term displacement from June 2016 to June 2021. Through the decomposition and reconstruction process, it was found that the optimal choice for L is 9, as it achieves the best results. This selection of L strikes a balance between capturing the trend and periodic components, making it the most ideal configuration. After the decomposition and reconstruction of the trend term and periodic term, it is the most ideal. When L selects 28, the reconstruction error is the smallest, but it is not conducive for the decomposition of reasonable

trends and periodic terms, and needs to be debugged back and forth. The small L often causes the sequence trend term and the periodic term to be mixed together. Selecting a larger L can often minimize random components hidden in the original signal, and very large L causes the singular value decomposition time to increase [2]. The number of singular values is determined to be 5 by infinite approximation of Fourier transform iterative experiment, and the first 4 groups are selected for reconstruction. When they are reconstructed, the fifth group of data are messy and non-periodic and considered to be a random sequence. Thus, they are eliminated. Finally, the trend term and the periodic term are obtained (Fig. 8).

SSA removes random parts, decomposes them into trend term and periodic term and then performs cumulative comparisons (Fig. 9). The trend term and periodic term reconstructed are evaluated with the actual displacement time series, and the reconstruction sequence is evaluated by MAE, MSE and R . The evaluation indicators are shown in Table 1.

4.2 Trend displacement prediction

From the SSA of Sect. 4.1, all monitoring points are selected for trend displacement extraction. The trend training and test are also programmed in pycharm, and then the polynomial expansion coefficient and power order are fitted and solved. Training data are taken from June 2016 to June 2020 (80%), and test data are taken from July 2020 to June 2021 (20%). At present, the trend term of landslide prediction is generally predicted by time step, because the trend term is affected by the internal potential factor, and the influencing factor is difficult to quantify. In previous landslide displacement predictions, most monitoring periods can last 5–10 years, and the monitoring interval is typically 1 month. That is, limited monitoring data is distributed over a long time span. In all the fitting methods, the decomposition of the sequence in Sect. 4.1 can be seen to increase the trend more stably. In extracting the trend term displacement using multiple fitting is better. Iterative approximation fitting helps to select the most reasonable power and number of items. The polynomial fitting is the

Table 5 Optimal SVR model parameters

	YY208			YY209			YY210		
	PSO	GSA	PSO-GSA	PSO	GSA	PSO-GSA	PSO	GSA	PSO-GSA
C	3.498	3.375	11.178	3168	3.605	9.704	5000	2.654	8.374
g	0.617	0.629	1.550	0.535	0.745	1.569	0.755	0.613	4.965

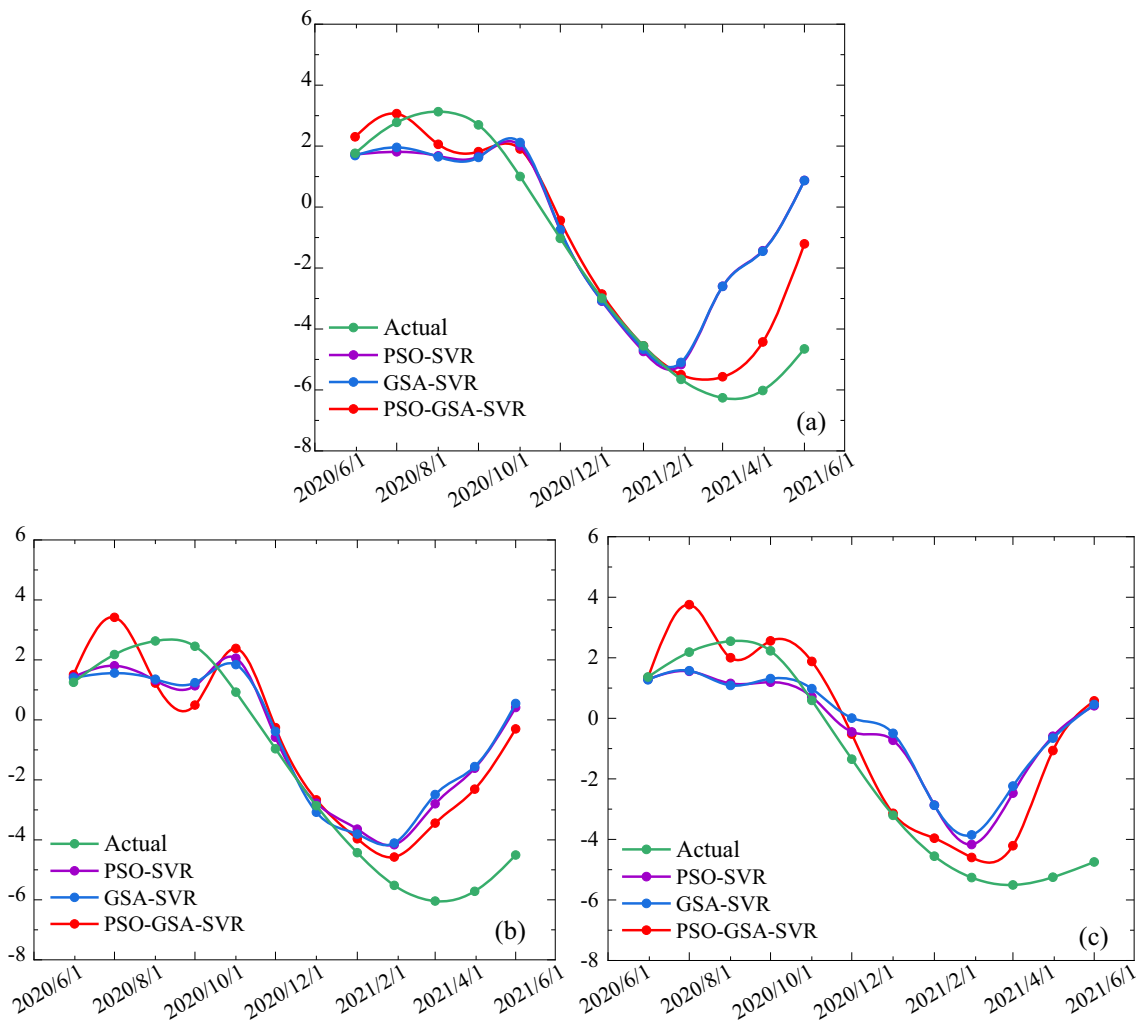


Fig. 12 Comparison of actual–predicted periodic displacement by different optimized models: **a** YY208, **b** YY209, **c** YY210

Table 6 Evaluation and error comparison of all optimized SVR models

	YY208			YY209			YY210		
	PSO	GSA	PSO-GSA	PSO	GSA	PSO-GSA	PSO	GSA	PSO-GSA
MSE (mm ²)	5.867	5881	5.357	4.923	5.217	3.935	6.000	6.364	5.244
MAE (mm)	1.603	1.587	1.374	1.599	1.645	1.560	1855	1.974	1.870
R	0.795	0.805	0.856	0.832	0.818	0.865	0.805	0.812	0.862

best after repeated attempts. The polynomial coefficients are shown in Table 2, and the fitting formula is shown in Eq. (13). The extracted trend items are fitted and trained, and the prediction results are obtained by the test data (Fig. 10). MAE, MSE and R evaluation indicators were used for the evaluation, as shown in the following equation and Table 3.

$$f(x) = a_0 + a_i \sum_1^i x^i \tag{13}$$

where a_0 and a_i is the expansion coefficient.

4.3 Periodic displacement prediction

4.3.1 Factor selection and evaluation

Rainfall: Rainfall is one of the triggering factors that leads to landslide deformation. During the infiltration-seepage process of rainfall, the stability of the landslide is destroyed by changing the soil pressure, matrix suction and

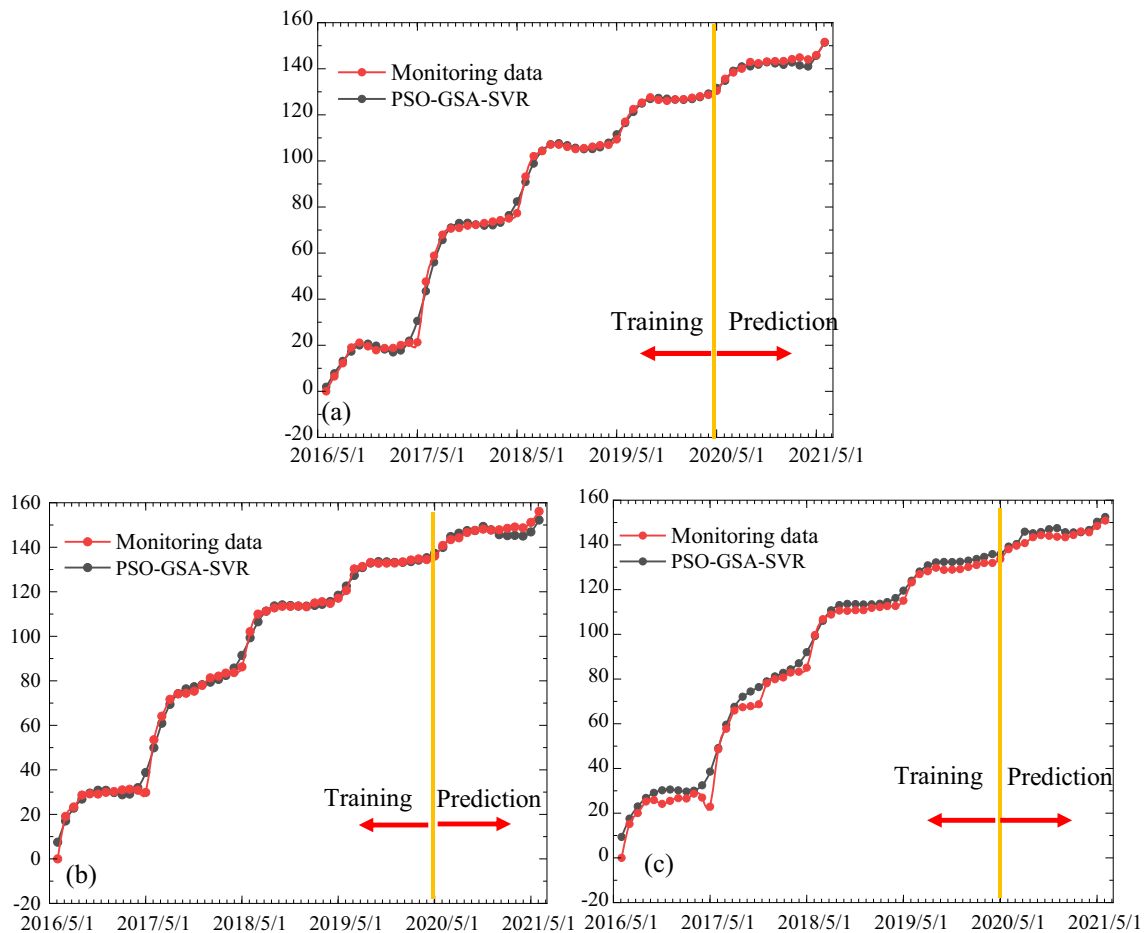


Fig. 13 Comparison of predicted–actual total displacement of each monitoring point: **a** YY208, **b** YY209, **c** YY210

Table 7 cumulative displacement and actual monitoring displacement accuracy and error

	YY208	YY209	YY210
MSE (mm ²)	6.043	6864	5.975
MAE (mm)	1.744	1.823	1.706
R	0.998	0.998	0.998

hydrodynamic pressure of the soil. This results in the deformation of the landslide. On the other hand, infiltration of rainfall in soil causes chemical reaction, and soil–water reaction leads to the reaction of mudding, softening and chemical dissolution of hydrophilic substances. Finally, it leads to the change of internal cohesion and internal friction angle of soil, which indirectly changes the stress–strain state. This is because rainfall infiltration-seepage is a slow process, including runoff rainwater. Therefore, rainfall during this month, rainfall during the last 1-month and rainfall during the last 2-months are the rainfall factors selected for evaluation (Fig. 11a).

RWL: RWL is the major triggering factor that leads to landslide deformation. The fluctuation of RWL affects the distribution of underground hydrodynamic stress field, which affects the reduction of soil strength and the weakening of permeability. The rise of RWL leads to the dynamic water pressure pointing to the landslide, and the dynamic water pressure caused by the rapid decline of water level changes sharply. The landslide is most vulnerable to instability at this moment. The influence of RWL depends on its fluctuation. The step-like mutation displacement of the wading landslide in the TGR is affected by the decline of RWL every year. At this moment, RWL elevation, RWL change in the last 1-month and RWL change in the last 2-months are the RWL factors selected for evaluation (Fig. 11b).

Displacement increase: Due to the annual stepwise change of the landslide, it has periodic change. Displacement during the last 1-year and displacement during the last 1-month are the influencing shadows selected for evaluation (Fig. 11c).

In order to verify the rationality of factor selection, the degree of geometric similarity of curves composed of two

or more sequences (sequences can be understood as factors or indicators in the system) is studied by using grey correlation degree. Table 4 shows the relationship between the displacement of the three monitoring points YY208, YY209, YY210 and the influencing factors. Resolution coefficient greater than 0.5 is considered to have a correlation, and that greater than 0.6 is considered to have a close relationship. It indicates that the selected factors are reasonable enough. Using grey correlation analysis (YY208, YY209 and YY210), the spatial location plays a significant role in the correlation with rainfall, RWL and displacement. Specifically, for the rainfall category, the highest correlation was observed with the rainfall from the previous month. In the case of RWL category, it was associated with the elevation of the RWL. As for the displacement category, it was primarily correlated with the displacement from the previous month. However, the magnitude of correlation varied depending on the spatial location.

4.3.2 Parameter optimization and displacement prediction

As a single optimization algorithm cannot solve the optimization problem of high-dimensional search space, an improved GSA is proposed, which combines the GSA with PSO algorithm. By manipulating the boundary and activating the stagnated particles in the new search space, the particles jump out of the local area to find the optimal solution. The training data are taken from June 2016 to June 2020 (80%), and the test data are taken from July 2020 to June 2021 (20%) (Fig. 11a). In this paper, the improved GSA-PSO-SVR model is used to develop the periodic displacement model. The influencing factor and the sample data are read together, the parameters are selected according to the fitness in the iterative process, and SVR is selected to train and test the model. MSE is used as the fitness function return value of SVR. The specific settings are as follows.

- (1) Optimal settings for PSO-GSA algorithm: the particle swarm population is 20, the maximum iteration is 100, the gravitational constant is 3, the reference function is [1, 10] learning factors $C1 = 0.5$, $C2 = 0.5$ and the optimal penalty function is found in Table 5
- (2) Optimal settings for PSO algorithm: the number of population is 20, the maximum iteration is 100, inertia weight $W = 1$, learning factor $C1 = 0.5$, $C2 = 0.5$, the optimal penalty function is found in Table 5
- (3) Optimal settings for GSA algorithm: the number of population is 20, the maximum iteration is 100, the gravitational constant is 3, the optimal penalty factor

and kernel function parameters are shown in Table 5. The optimal penalty factor C and kernel function g are used to train and predict the samples

Compared with the prediction results of PSO, GSA and PSO-GSA (Fig. 12), the accuracy and error of each model are shown in Table 6. In terms of the goodness of fit, employing a hybrid optimized SVR approach resulted in an average improvement of 5% in the R . Additionally, both MAE and MSE were reduced to some extent. This indicates that by sufficiently optimizing the model, it is possible to enhance its predictive performance. Further analysis shows that the PSO-GSA-SVR prediction model works best as the final periodic displacement prediction model.

4.4 Cumulative displacement prediction and evaluation

Based on the time cumulative sequence observed in Eq. (10), the total predicted displacement is to add the trend term and the periodic term using PSO-GSA-SVR model. From Fig. 10 and 12, the corresponding predicted displacements of the three monitoring points from June 2016 to June 2021 can be obtained, and the predicted displacements are compared with the actual monitoring displacement values (Fig. 13). According to the error calculation and accuracy evaluation, it is concluded that the change trend is consistent with the actual situation. MSE and MAE are smaller, and the correlation coefficient R is relatively larger (in Table 7). It has engineering application prospects and predicts short-term displacement changes.

5 Conclusion

This paper proposed the hybrid optimization algorithm-based displacement prediction model. Taking Jiuxianping wading rock landslide with obvious step-like displacement as an example, three monitoring displacement points are selected for modeling and validation. The major contributions of this study are as follows:

- (1) The periodicity of RWL affects the step-like distribution of landslide displacement, and the rise of RWL makes the landslide displacement to change steadily. Under the combined action of low RWL and rainstorm, the landslide displacement shows obvious step-like characteristic. RWL is the major factor that induced the landslide deformation. RWL below 160 m is prone to cause landslide disaster, followed by rainfall, which accelerates landslide deformation tendency

- (2) Due to the influence of SSA in short-term power load and medical results, the introduction of SSA is applicable. SSA in time series decomposition is model-free, parameter-free and does not require stationary time series. It has a good performance in decomposing the nonlinear step-like landslide displacement. The reconstructed sequence error is small after removing the random term. The MSE and MAE of the prediction model of the decomposed periodic term are small, and the correlation coefficient is high
- (3) The selected three monitoring points YY208, YY209 and YY210 have obvious step-like state, and the small sample data are collected once a month. Using the hybrid optimization coupled SVR model, the predicted total displacement of the three monitoring points has small MSE and MAE. It shows that the improved PSO-GSA has good optimization characteristics and can activate the stagnated particles to jump out of the local area. It also shows that SVR has enough advantages in solving the problem of small sample and high dimension nonlinear regression

As the displacement of Jiuxianping landslide is analyzed once in a month as well as its sample size, the improved GSA-PSO-SVR model is applied to predict the displacement of Jiuxianping landslide in the TGR area. It is reliable and has great engineering referencing significance.

Funding Natural Science Foundation of Chongqing, Award Number: CSTB2022NSCQ-MSX0594.

Data availability All data, or codes generated or used during the study are available from the corresponding author upon request.

Declarations

Conflict of interest The authors declare no competing interests.

References

1. Cao Y, Yin KL, Alexander DE, Zhou C (2015) Using an extreme learning machine to predict the displacement of step-like landslides in relation to controlling factors. *Landslides* 13(4):725–736. <https://doi.org/10.1007/s10346-015-0596-z>
2. Dai AM, Xu AQ, Sun WC (2016) Signal denoising method based on improve singular spectrum analysis. *Trans Beijing Inst Technol* 36(7):727–732+759
3. Dong DM, Liang Y, Wang LQ, Wang CS, Sun ZH, Wang C, Dong MM (2017) Displacement prediction method based on ensemble empirical mode decomposition and support vector machine regression—a case of landslides in three Gorges reservoir area. *Rock Soil Mech* 38(12):3660–3669. <https://doi.org/10.16285/j.rsm.2017.12.034>
4. Du J, Yin KL, Lacasse S (2013) Displacement prediction in colluvial landslides, three Gorges reservoir, China. *Landslides* 10:203–218. <https://doi.org/10.1007/s10346-012-0326-8>
5. Gao SC, Vairappan C, Wang Y, Cao QP, Tang Z (2014) Gravitational search algorithm combined with chaos for unconstrained numerical optimization. *Appl Math Comput* 231:48–62. <https://doi.org/10.1016/j.amc.2013.12.175>
6. Golyandina N, Korobeynikov A (2014) Basic singular spectrum analysis and forecasting with R. *Comput Stat Data Anal* 71:934–954. <https://doi.org/10.1016/j.csda.2013.04.009>
7. Han HM, Shi B, Zhang L (2021) Prediction of landslide sharp increase displacement by SVM with considering hysteresis of groundwater change. *Eng Geol*. <https://doi.org/10.1016/j.enggeo.2020.105876>
8. Hassani H, Ghodsi Z (2015) A glance at the applications of variational spectrum analysis in gene expression data. *Biomol Detect Quantif* 4:17–21. <https://doi.org/10.1016/j.bdq.2015.04.001>
9. He FF, Zhou JZ, Zhong-kai F, Liu GB, Yang YQ (2019) A hybrid short-term load forecasting model based on variational mode decomposition and long short-term memory networks considering relevant factors with Bayesian optimization algorithm. *Appl Energy* 237:103–116. <https://doi.org/10.1016/j.apenergy.2019.01.055>
10. Hong HY, Pourghasemi HR, Pourtaghi ZS (2016) Landslide susceptibility assessment in Lianhua county (China): a comparison between a random forest data mining technique and bivariate and multivariate statistical models. *Geomorphology* 259:105–118. <https://doi.org/10.1016/j.geomorph.2016.02.012>
11. Jiang Q, Jiao YY, Song L, Wang H, Xie BT (2019) Experimental study on reservoir landslide under rainfall and water-level fluctuation. *Rock Soil Mech* 40(11):4361–4370. <https://doi.org/10.16285/j.rsm.2018.1617>
12. Jiang YH, Wang W, Zou LF, Wang RB, Liu SF, Dun LL (2022) Research on dynamic prediction model of landslide displacement based on PSO-VMD, NARX and GRU. *Rock Soil Mech* 43(S1):1–12. <https://doi.org/10.16285/j.rsm.2021.0247>
13. Jiao YY, Song L, Tang HM (2014) Material weakening of slip zone soils induced by water level fluctuation in the ancient landslides of three Gorges reservoir. *Adv Mater Sci Eng* 2014:1–9. <https://doi.org/10.1155/2014/202340>
14. Lian C, Zeng ZG, Yao W, Tang HM (2013) Displacement prediction model of landslide based on a modified ensemble empirical mode decomposition and extreme learning machine. *Nat Hazards* 66(2):759–771. <https://doi.org/10.1007/s11069-012-0517-6>
15. Lian C, Zeng ZG, Yao W, Tang HM (2015) Multiple neural networks switched prediction for landslide displacement. *Eng Geol* 186:91–99. <https://doi.org/10.1016/j.enggeo.2014.11.014>
16. Liao K, Wu YP, Miao FS, Li LW, Xue Y (2020) Using a kernel extreme learning machine with grey wolf optimization to predict the displacement of step-like landslide. *Bull Eng Geol Environ* 79:673–685. <https://doi.org/10.1007/s10064-019-01598-9>
17. Liu ZB, Shao JF, Xu WY, Chen HJ, Shi C (2014) Comparison on landslide nonlinear displacement analysis and prediction with computational intelligence approaches. *Landslides* 11:889–896. <https://doi.org/10.1007/s10346-013-0443-z>
18. Liu H, Mi XW, Li YF (2018) Smart multi-step deep learning model for wind speed forecasting based on variational mode decomposition, singular spectrum analysis, LSTM network and ELM. *Energy Convers Manag* 159:54–64. <https://doi.org/10.1016/j.enconman.2018.01.010>
19. Liu SL, Wang LQ, Zhang WG, He YW, Pijush S (2023) A comprehensive review of machine learning-based methods in landslide susceptibility mapping. *Geol J*. <https://doi.org/10.1002/gj.4666>

20. Long JJ, Li CD, Liu Y, Feng PF, Zuo QJ (2022) A multi-feature fusion transfer learning method for displacement prediction of rainfall reservoir-induced landslide in three Gorges reservoir area based on H-P filter, ARIMA and VAR models. *Rock Soil Mech* 37(S2):552–560. <https://doi.org/10.16285/j.rsm.2016.S2.070>
21. Meng M, Chen ZQ, Huang D, Zeng B, Cheng CJ (2016) Displacement prediction of landslide in three Gorges reservoir area based on H-P filter, ARIMA and VAR models. *Rock Soil Mech* 37(S2):552–560. <https://doi.org/10.16285/j.rsm.2016.S2.070>
22. Miao FS, Wu YP, Xie YH, Li YN (2018) Prediction of landslide displacement with step-like behavior based on multialgorithm optimization and a support vector regression model. *Landslides* 15:475–488. <https://doi.org/10.1007/s10346-017-0883-y>
23. Miao FS, Wu YP, Xie YH, Li YN, Li LW (2018) Centrifugal test on retrogressive landslide influenced by rising and falling reservoir water level. *Rock Soil Mech* 39(2):605–613. <https://doi.org/10.16285/j.rsm.2016.2518>
24. Phoon K, Zhang WG (2022) Future of machine learning in geotechnics. *Georisk: Assess Manag Risk Eng Syst Geohazards* 17(1):7–22. <https://doi.org/10.1080/17499518.2022.2087884>
25. Schoellhamer DH (2001) Singular spectrum analysis for time series with missing data. *Geophys Res Lett* 28(16):3187–3190. <https://doi.org/10.1029/2000GL012698>
26. Tang HM (2022) Advance and prospect on prediction and forecasting of major landslides. *Bull Geol Sci Technol* 41(6):1–13
27. Wang JN, Li XT (2011) An improved gravitation search algorithm for unconstrained optimization. *Adv Mater Res* 143:409–413. <https://doi.org/10.4028/www.scientific.net/AMR.143-144.409>
28. Wen HJ, Zhang YY, Fu HM (2018) Research status of instability mechanism of rainfall-induced landslide and stability evaluation methods. *China J Highw Transp* 31(2):15–31
29. Wen HJ, Xiao JF, Wang XF, Xiang XK, Zhou XZ (2023) Analysis of soil-water characteristics and stability evolution of rainfall-induced landslide: a case of the Siwan village landslide. *Forests* 14(4):808. <https://doi.org/10.3390/f14040808>
30. Wen HJ, Li WL, Xu C, Daimaru H (2023) Landslides in forests around the world: causes and mitigation. *Forests* 14(3):629. <https://doi.org/10.3390/f14030629>
31. Wen HJ, Zhou XZ, Zhang C, Liao MY, Xiao JF (2023) Different-classification-scheme-based machine learning model of building seismic resilience assessment in a mountainous region. *Remote Sens* 15(9):2226. <https://doi.org/10.3390/rs15092226>
32. Wu SS, Hu XL, Zheng WB (2021) Effects of reservoir level fluctuations and rainfall on a landslide by two-way ANOVA and K-means clustering. *Bull Eng Geol Env* 80(7):5405–5421. <https://doi.org/10.1007/s10064-021-02273-8>
33. Yang XH, Zhou TY, Diao XF, Hu F, Long XY (2022) A model test of accumulation landslide under the coupling effect of river erosion and rainfall. *J Lanzhou Univ (Nat Sci)* 58(4):483–491
34. Yin YP, Huang BL, Wang WP (2016) Reservoir-induced landslides and risk control in three Gorges project on Yangtze river, China. *J Rock Mech Geotech Eng* 8(5):577–595. <https://doi.org/10.1016/j.jrmge.2016.08.001>
35. Zhang J, Yin KL, Wang JJ, Huang FM (2015) Displacement prediction of Baishuihe Landslide based on time series and PSO-SVR model. *Chin J Rock Mech Eng* 34(2):382–391
36. Zhang XB, Wang JZ, Zhang KQ (2017) Short-term electric load forecasting based on singular spectrum analysis and support vector machine optimized by Cuckoo search algorithm. *Electr Power Syst Res* 146:270–285. <https://doi.org/10.1016/j.epsr.2017.01.035>
37. Zhang YY, Wen HJ, Ma CC (2018) Failure mechanism and stability analysis of huge landslide of Caijiaba based on multi-source data. *Chin J Rock Mech Eng* 37(9):2048–2063
38. Zhang YG, Tang J, He ZY, Tan JK, Li C (2021) A novel displacement prediction method using gated recurrent unit model with time series analysis in the Erdaohe landslide. *Nat Hazards* 105:783–813. <https://doi.org/10.1007/s11069-020-04337-6>
39. Zhang WG, Li HR, Tang LB, Gu X, Wang LQ, Wang L (2022) Displacement prediction of Jiuxianping landslide using gated recurrent unit (GRU) networks. *Acta Geotech* 14(4):1367–1382. <https://doi.org/10.1007/s11440-022-01495-8>
40. Zhang WG, Li HR, Han L, Chen LL, Wang L (2022) Slope stability prediction using ensemble learning techniques: a case study in Yunyang county, Chongqing, China. *J Rock Mech Geotech Eng* 14(4):1089–1099. <https://doi.org/10.1016/j.jrmge.2021.12.011>
41. Zhang C, Wen HJ, Liao MY, Lin Y, Wu Y, Zhang H (2022) Study on machine learning models for building resilience evaluation in mountainous area: a case study of Banan district, Chongqing, China. *Sensors* 22(3):1163. <https://doi.org/10.3390/s22031163>
42. Zhang WG, Wu CZ, Tang LB, Gu X, Wang L (2022) Efficient time-variant reliability analysis of Bazimen landslide in the three Gorges Reservoir area using XGBoost and LightGBM algorithms. *Gondwana Res*. <https://doi.org/10.1016/j.gr.2022.10.004>
43. Zhang WG, Gu X, Tang LB, Yin YP, Liu DS, Zhang YM (2022) Application of machine learning, deep learning and optimization algorithms in geoenvironment and geoscience: comprehensive review and future challenge. *Gondwana Res* 109:1–17. <https://doi.org/10.1016/j.gr.2022.03.015>
44. Zhang JY, Ma XL, Zhang JL, Sun DL, Zhou XZ, Mi CL, Wen HJ (2023) Insights into geospatial heterogeneity of landslide susceptibility based on the SHAP-XGBoost model. *J Environ Manag* 332:117357. <https://doi.org/10.1016/j.jenvman.2023.117357>
45. Zhou C, Yin KL, Cao Y, Ahmed B (2016) Application of time series analysis and PSO-SVM model in predicting the Bazimen landslide in the three Gorges Reservoir, China. *Eng Geol* 204:108–120. <https://doi.org/10.1016/j.enggeo.2016.02.009>
46. Zhou XZ, Wen HJ, Zhang YL, Xu JH, Zhang WG (2021) Landslide susceptibility mapping using hybrid random forest with GeoDetector and RFE for factor optimization. *Geosci Front* 12(5):101211. <https://doi.org/10.1016/j.gsf.2021.101211>

Publisher's Note Springer Nature remains neutral with regard to jurisdictional claims in published maps and institutional affiliations.

Springer Nature or its licensor (e.g. a society or other partner) holds exclusive rights to this article under a publishing agreement with the author(s) or other rightsholder(s); author self-archiving of the accepted manuscript version of this article is solely governed by the terms of such publishing agreement and applicable law.